Supporting Information for "Limits on runoff episode duration for early Mars: integrating climate models and lake hydrology"

Gaia Stucky de Quay[1,2], Timothy A. Goudge[1,2], Edwin S. Kite[3], Caleb I. Fassett[4], and Scott D. Guzewich[5]

[1]Jackson School of Geosciences, University of Texas at Austin, Austin, Texas 78712, USA

[2]Center for Planetary Systems Habitability, University of Texas at Austin, Austin, Texas 78712, USA

[3]Department of the Geophysical Sciences, University of Chicago, Chicago, Illinois 60637, USA

[4]NASA Marshall Space Flight Center, Huntsville, Alabama 35805, USA

[5]NASA Goddard Space Flight Center, Greenbelt, Maryland 20771, USA

Corresponding author: G. Stucky de Quay, (g.stucky@utexas.edu)

Contents of this file

Introduction

This Supporting Information (SI) document contains additional information on assumptions made during mapping of open- and closed-basin lakes (Text S1). It also describes the effects of sedimentary infill on our results (Text S2). Then, it provides a full derivation of the volumetric and timescale functions presented in equations (2) – (4) in the main text (Text S3). Further, the SI contains a schematic overview of the early Mars climate and the relevant parameters used in this study (Figure S1), maps of the coupled lake systems (Figure S2), as well as modified results from Figure 4 assuming a climate regime with no evaporation (Figure S3) and modified results if we reduce the population of coupled systems following Text S1 (Figures S4 and S5). Finally, the SI provides four tables (Tables S1-S4): Table S1 lists additional information for studies shown in Figure 1, Table S2 summarizes data that are available for 8 studies (4 geomoprhic analyses + 4 climate models), Table S3 presents our full database of coupled lake systems and their morphometric parameters, and Table S4 summarizes the climate model scenarios used for Figure 4 (and Figures S3,S5).

Text S1. Identification of open- vs. closed-basin lakes

Open- and closed- basin lakes were classified based on whether or not they contained an outlet canyon. Although it is possible some overflow may have occurred without visible outlet canyon erosion, we interpret the lack of geologic evidence for overflow as an indication that the lake system was closed (Supplementary Figure S2). However, because the craters we interpret as closed basins may have been modified by later processes, the lack of an observed outlet is not definitive proof that one never formed. Based on contextual evidence, however, the odds that more than 1-2 of the basins we interpret as closed overflowed is low. Further, the observation that closed-basin lakes always allow greater water inputs (smaller areas, larger basins) than their coupled open-basin lake counterparts is in line with the assumption that they were not breached.

Stucky de Quay et al. (2020) showed that removal of closed-basin lakes with depressions on their rims (potential outflows that did not form defined canyons) did not affect distributions of hydrologic reconstructions. Here we apply a similar modification to our results and remove two systems from our analyses that could arguably be of reduced confidence: Basin IDs 47/13 and 231/216 (see Supplementary Table S3; Figure S2). Recalculation of results using the 5 remaining coupled systems (as shown originally in Figures 2e,f and 4 in the main text) are shown in Supplementary Figures S4 and S5. These results show that the removed basins lie within the range of our original population, and thus do not affect our overarching quantitative findings: the range of T_{max}/T_B values in Figures 2e,f ($1.6 - 63$) or the range of episode runoff durations in Figure 4 ($10^2 - 10^5$ yr).

Text S2. Basin infill and sedimentary volume considerations

Here we consider various infilling scenarios—depending on when they occur—and how they may (or may not) affect our results.

First, although the morphology of basins indicates they have been significantly infilled (e.g., flat crater floors in Figure 2a and Figures S2a-f), the majority of this infill would have occurred prior to the valley network era (i.e., during the Noachian period; Malin & Edgett, 2000; Craddock et al., 2002). As such, this infill occurred before our valley network-fed runoff events and do not affect our results. Subsequently, during the valley network period, sediment may also have been eroded from the valley network watersheds (from both open- and closed-basin lakes) and deposited into the basins for any episode preceding the breaching runoff episode (e.g., any of the episodes before breaching episode in Figure S1a indicated by (i)). This sediment volume would not affect our results because it was deposited prior to the breaching episode, and our measured lake volumes exclude this sediment volume.

Second, sediment may be added to the basins during the breaching runoff episode (breaching episode in Figure S1a, (ii)). This sediment could be derived from either inlet incision (from both open- and/or closed basin lake watersheds) and/or outlet canyon incision (deposited in the downstream closed-basin lake). In both cases, this sedimentary infill will not affect our results because we are only concerned with basin water volumes at the end of runoff episode. In other words, any sediment volume that is eroded, transported, and deposited in the basin at any point within the breaching runoff episode *remains* in the basin up to the present—thus, when we measure lake volumes using present-day topography, the sediment volumes are not incorporated in our lake volumes. In this

way, our lake volumes consider only the water volume and are not affected by synfluvial sedimentation during the breaching episode.

Third, infill may occur after the breaching runoff episode. This could either be due to (a) subsequent runoff episodes (i.e., if there are many more runoff episodes after the breaching episode; Figure S1a, (iii)), or (b) postfluvial processes such as aeolian deposition. Although these would have an impact on our results, they are unlikely to significantly modify our volume estimates, as we explain below. To assess the maximum value of the first contribution, let us make the assumption that the breaching episode is the very first runoff episode to occur in a series of episodes (e.g., the breaching episode is the first peak in Figure S1a). This would mean that approximately the entire eroded watershed volume (measured from the inlets) would be deposited into the basin after our breaching event, resulting in our measured lake volumes being an underestimate. For Jezero crater, the eroded volume from the watershed is $\sim$58 km^3 (Fassett and Head, 2005). The basin volume is $\sim$424 km^3 (see Open Basin ID 45 from Stucky de Quay et al., 2020). This would mean the basin volume before sediment deposition from inlets would have been 482 km^3, i.e., only 14% greater. For the second contribution, aeolian deposits are likely to be a few tens of meters (e.g., dust mantle thickness of $\sim$20 m from Mangold et al., 2009) and would only infill $\sim$10% of the basins, which are on average $\sim$200 m deep (Stucky de Quay et al., 2020). As such, even if we sum up both liberal contributions, paleolake volumes could only have been up to $\sim$24% larger, which would change episode duration values by the same proportion, and thus not significantly alter our results.

In summary, sediment deposition into the basins occurring before or during the breaching runoff episode does not affect our lake volume calculations, and sediment deposition

occurring after the breaching runoff episode (whether through fluvial or aeolian processes) is not significant relative to the size of the basin.

Text S3. Full derivation of lake hydrology and timescale expressions

Open-basin lake. In an embedded lake system, where an open-basin lake is located within the watershed of a closed-basin lake, the changes in lake volume over time can be calculated using a simple model. The following derivation of this expression builds on the standard hydrological balance in equation (1) to derive the final expression for lake volumes in equations (2) and (3) in the main text.

For an open-basin lake (O), the volume of water, v_O within its basin as a function of time, t, before breaching (and excluding any losses; discussed further later) can be expressed as

$$v_O[t \leq T_B] = (A_{L,O} + A_{W,O})P \times t, \tag{6}$$

assuming a steady precipitation rate, P, across the lake area, $A_{L,O}$ and watershed area $A_{W,O}$. When the volume of water within open-basin lake reaches the maximum volume held by the basin, i.e., $v_O = V_{L,O}$, then the lake breaches. When this event occurs at a time $t = T_B$, the lake overflows and causes catastrophic canyon erosion (Fassett & Head, 2008; Goudge et al., 2019). Due to the lowered outlet canyon floor, some water drains from the open-basin lake into the downstream closed basin lake. The remaining volume of water in the basin contained after breaching is given by V_R. Since the open- and closed-basin lakes are now hydrologically connected—and the open-basin lake volume remains steady at V_R—any additional water input to this volume is not topographically contained and would be transferred downstream. We can now express these two time-dependent states as a piece-wise function:

$$v_O = \begin{cases} (A_{L,O} + A_{W,O})Pt & \text{if } t \leq T_B; \\ V_R & \text{if } t > T_B; \end{cases} \tag{7}$$

This function describes how the lake volume changes as a function of t, given the measured morphometric parameters $A_{L,O}$, $A_{W,O}$, and V_R, and a known P. Below we derive a similar, expression for the closed-basin lake.

Closed-basin lake. For a closed-basin lake (C) in an embedded coupled system, the changes in lake volume can also be broken down into before and after open-basin lake breaching. Before the breach at T_B, the closed-basin lake is not connected to the upstream open-basin lake, and so the volume of water that accumulates in the basin, again excluding losses, is simply proportional to the combined watershed and lake areas, analogous to equation (6):

$$v_C[t \leq T_B] = (A_{L,C} + A_{W,C})P \times t. \tag{8}$$

However, after the open-basin lake breach two key events occur. First, the drained volume in the upstream open-basin lake is transferred to the closed-basin lake; we assume this to be instantaneous following a catastrophic erosion event (Goudge et al., 2019). Second, the closed-basin system has now captured the watershed of the upstream open-basin lake, such that the contributing watershed now consists of both watersheds. This means that the volume of a closed-basin after T_B consists of three terms: (i) the total volume accumulated from equation (8) up to the breach, $(A_{L,C} + AW, C)PT_B$, (ii) the transferred water volume from upstream lake overflow and outlet canyon erosion, $V_{L,O} - V_R$, and (iii) the new rate of volume accumulation from the combined watersheds after breaching, $(A_{L,O} + A_{W,O} + A_{L,C} + A_{W,C})P(t - T_B)$. We can thus express the post-breach volume of a closed-basin lake as the total sum of these terms, such that

$$v_C[t > T_B] = (A_C P T_B) + (V_{L,O} - V_R) + (A_{L,O} + A_{W,O} + A_{L,C} + A_{W,C})P(t - T_B). \tag{9}$$

By expanding the third term and canceling out repeated terms, equation (9) can be written as

$$v_C[t > T_B] = V_{L,O} - V_R + (A_{L,O} + A_{W,O} + A_{L,C} + A_{W,C})Pt - (A_{L,O} + A_{W,O})PT_B. \quad (10)$$

In order to simplify this, we substitute the term for the open-basin lake volume at T_B. The open-basin lake volume v_O is equal to $V_{L,O}$ when $t = T_B$. Hence, we can rewrite equation (6) as

$$V_{L,O} = (A_{L,O} + A_{W,O})PT_B. \quad (11)$$

Since this is equivalent to the final term in equation (10), we substitute equation (11) into equation (10), which, after simplifying, results in

$$v_C[t > T_B] = (A_{L,O} + A_{W,O} + A_{L,C} + A_{W,C})Pt - V_R. \quad (12)$$

Similarly to equation (7), we express the volume of a closed-basin lake as a function of time, using piece-wise functions built from equation (8) and (12):

$$v_C = \begin{cases} (A_{L,C} + A_{W,C})Pt & \text{if } t \leq T_B; \\ \\ (A_{L,O} + A_{W,O} + A_{L,C} + A_{W,C})Pt - V_R & \text{if } t > T_B; \end{cases} \quad (13)$$

As a result, we now have two sets of equations, (7) and (13), which describe open- and closed-basin lake volumes, respectively, as a function of time, both before and after open-basin lake breaching. However, both of these expressions require knowledge of a precipitation rate, P. Since both open- and closed-basin lakes are spatially coincident, and thus it is safe to assume they experience the same precipitation rate, we can remove the precipitation term by normalizing both expressions, obtaining lake volume expressions as a function of relative time (see below).

Normalization. In order to solve for lake volumes as a function of relative time, we remove the P dependency from equations (7) and (13). To do this, we can take equation (11), which defines the open-basin lake volume at the time of breach, and rearrange it so that we instead obtain a definition for P:

$$P = \frac{V_{L,O}}{(A_{L,O} + A_{W,O})T_B}. \tag{14}$$

Since the precipitation rate is assumed to be the same for both open- and closed-basin lakes, we substitute equation (14) into the precipitation term in equations (7) and (13). This means that Pt can now be expressed as $\frac{V_{L,O}}{A_{L,O}+A_{W,O}}\left(\frac{t}{T_B}\right)$; this allows the volume expressions to be a function of time relative to breaching, i.e., $v = f\left(\frac{t}{T_B}\right)$. This substitution results in the following expressions:

$$v_O = \begin{cases} V_{L,O}\left(\dfrac{t}{T_B}\right) & \text{if } t \leq T_B; \\ V_R & \text{if } t > T_B; \end{cases} \tag{15}$$

$$v_C = \begin{cases} (A_{L,C} + A_{W,C})\dfrac{V_{L,O}}{A_{L,O} + A_{W,O}}\left(\dfrac{t}{T_B}\right) & \text{if } t \leq T_B; \\ (A_{W,O} + A_{L,O} + A_{L,C} + A_{W,C})\dfrac{V_{L,O}}{A_{L,O} + A_{W,O}}\left(\dfrac{t}{T_B}\right) - V_R & \text{if } t > T_B. \end{cases} \tag{16}$$

Note that the volume expressions are essentially normalized to the morphology of the open-basin lake. Equations (15) and (16) are similar to equations (2) and (3) in the main text, but do not take into account losses due to evaporation, for which our approach is described below.

Evaporation losses. Thus far, equations (6)-(16) do not consider the effects of evaporation on lake volumes. Equation (1) in the main texts shows that evaporation is assumed to occur over the lake area. Note that we assume here all precipitation from the water-

shed ends up in the lake, whether through surface runoff or infiltration and subsequent re-emergence into the valleys or the lake. Stucky de Quay et al. (2020) investigated how losses from the watershed affected the water balance, showing that even a 50% fractional loss (where half of the precipitation incident on the watershed is lost) results in limited changes to the overall hydrological reconstruction of the lake system. As such, the only lake loss explicitly considered in this study is evaporation from the lake surface.

In order to take into account losses due to lake evaporation, we can express evaporation as a fraction of the precipitation. One way to do this is using the aridity index, AI, which is simply the ratio of precipitation to evaporation ($\mathrm{AI} = P/E$). Another, related term, is the X ratio defined in Howard (2007), which is given as $X = (E - P)/P$, if we assume that all the precipitation ends up in the lake as described above. Note that both values are interchangeable, as $X = 1/\mathrm{AI} - 1$. The aridity index benefits from being a common parameter that can be easily compared to terrestrial values; however, the X ratio results in a more simplified balance expression. For instance, when using the aridity index as a substitute for the evaporative term, equation (1) becomes

$$V_L = ((A_W + A_L)P - (A_L)\frac{P}{\mathrm{AI}})T, \tag{17}$$

whereas the same equation expressed using the X ratio would take the form

$$V_L = (A_W - XA_L)PT. \tag{18}$$

Due to the simplicity of equation (18) relative to equation (17), we favor the X ratio for display purposes. In a system with no evaporation, the aridity index is infinite, and the X ratio is -1. For this study we use a semiarid scenario as proposed in Stucky de Quay et al., (2020), where open-basin lakes need a minimum global aridity index $\mathrm{AI} \simeq 0.26$ to

overflow (consistent with the semiarid hydrological regime required by Matsubara et al., 2011). This value is the most arid scenario that allows all open-basin lakes on Mars to exist. Timescale results in Figure 3b, Figure 4, and Figure S1, consider two end-member scenarios: no evaporation and AI = 0.26. Adding the evaporative terms in equation (18) to equations (15) and (16) results in the final equations (2) and (3) in the main text. Finally, to calculate the values plotted in Figures 3b,c, we normalize equations (2) and (3) by the volume of the closed-basin lake, i.e., both sides of both equations are divided by $V_{L,C}$. This allows all the plots to have maximum permitted normalized volumes < 1.

Embedded vs. Adjacent systems. The expressions derived thus far are only applicable to embedded coupled systems, i.e., systems wherein some lake overflow volume from the open-basin lake is transferred directly (and instantaneously) to the closed-basin lake, and where the closed-basin lake captures the watershed of the open-basin lake. However, one out of our seven mapped coupled systems is not embedded (Table S1), and is instead classified as an adjacent coupled system. These systems share significant drainage divides and are also assumed to be formed synchronously, with the main difference to embedded systems being that the outlet canyon does not flow into the closed-basin lake. For the case of our one adjacent system, $v_O = f(t/T_B)$ remains the same, but equation (3) takes the simpler, modified form:

$$v_C = (A_{W,C} - XA_{L,C})\frac{V_{L,O}}{A_{W,O} - XA_{L,O}}\left(\frac{t}{T_B}\right), \tag{19}$$

for all values of $\frac{t}{T_B}$ (i.e., independent of breaching), and where $v_C < V_{L,C}$. For our unique coupled system (Basin ID 171/140; Table S1), we use equation (19) instead of (3). Note that Figure 3b,c only includes the 6 embedded systems, and not the adjacent system,

since it does not follow the schematic behavior presented in Figure 3a.

Timescales. In addition to investigating lake volumes change with respect to relative timescales, we also derive expressions to solve for the absolute runoff episode duration lengths permitted. By rearranging equation (14), we can obtain an expression for T_B, such that

$$T_B = \frac{V_{L,O}}{(A_{L,O} + A_{W,O})P}. \tag{20}$$

Since the breaching timescale is the minimum timescale permitted to allow for the open-basin lake to breach, T_B, we combine this with the evaporation loss term in equation (18) to obtain the equation (4) presented in the main text. Conversely, for the maximum timescale for an embedded couple system, we take equation (12) and find the maximum volume permitted, $v_C = V_{L,C}$, and set $t = T_{max}$, such that

$$V_{L,C} = (A_{L,O} + A_{W,O} + A_{L,C} + A_{W,C})PT_{max} - V_R. \tag{21}$$

We then use the same evaporation expression from equation (18), and rearrange to solve for T_{max}, resulting in equation (5) in the main text. For our adjacent coupled system, equation (21) takes the simpler form:

$$V_{L,C} = (A_{L,C} + A_{W,C})PT_{max}, \tag{22}$$

as it has no dependency on the open-basin lake morphology. Accounting for evaporative losses, this results in the following expression for T_{max} as recorded by adjacent coupled systems:

$$T_{max} = \frac{V_{L,C}}{(A_{W,C} - XA_{L,C})P}, \tag{23}$$

analogous to equation (5) in the main text.

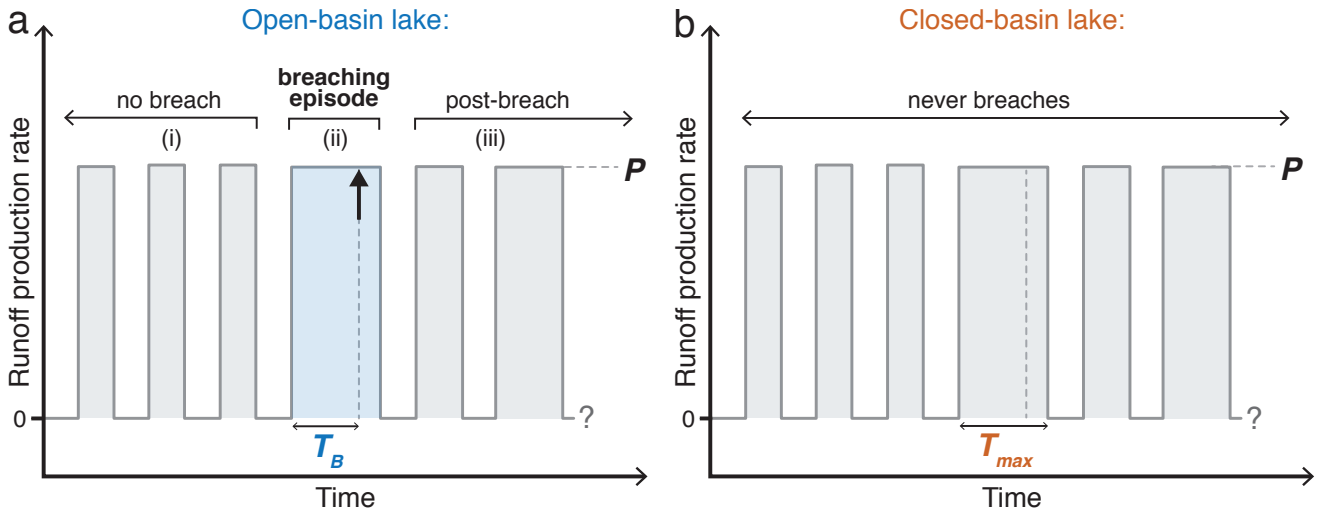

Figure S1. Schematic oscillating climate for late Noachian / early Hesperian Mars (>3.7 Ga), with variable runoff production rate over time (modified from Figure S1 in Stucky de Quay et al., 2020). Note that episodic runoff may be sourced from rainfall or snowmelt (e.g., Kite et al., 2013; Kite, 2019). In a coupled lake system, the (a) open-basin lake breaches (= black arrow) if a given runoff episode is sufficiently continuous, i.e., the duration exceeds T_B, and enough liquid water is supplied (where P is the time-averaged runoff rate). We term this episode the 'breaching runoff episode' (= light blue shaded box; (ii)). However, within the same coupled system, the (b) closed-basin lake never breaches. Thus, we can estimate maximum runoff episode duration, T_{max}, for a given runoff rate, P, from climate model outputs. In this work we quantify T_B and T_{max} for the breaching runoff episode of each coupled system. Importantly, episode durations before the breaching episode (see (i)) must always be less than T_B, but can be longer or shorter after the breaching episode (see (iii)). No episode duration can ever be greater than T_{max} (as this would cause the closed-basin lake to breach). Note that to erode the deep valley networks which feed these coupled systems, water volumes greatly exceeding lake volumes are required, suggesting multiple runoff events likely occurred (see Discussion section in the main text).

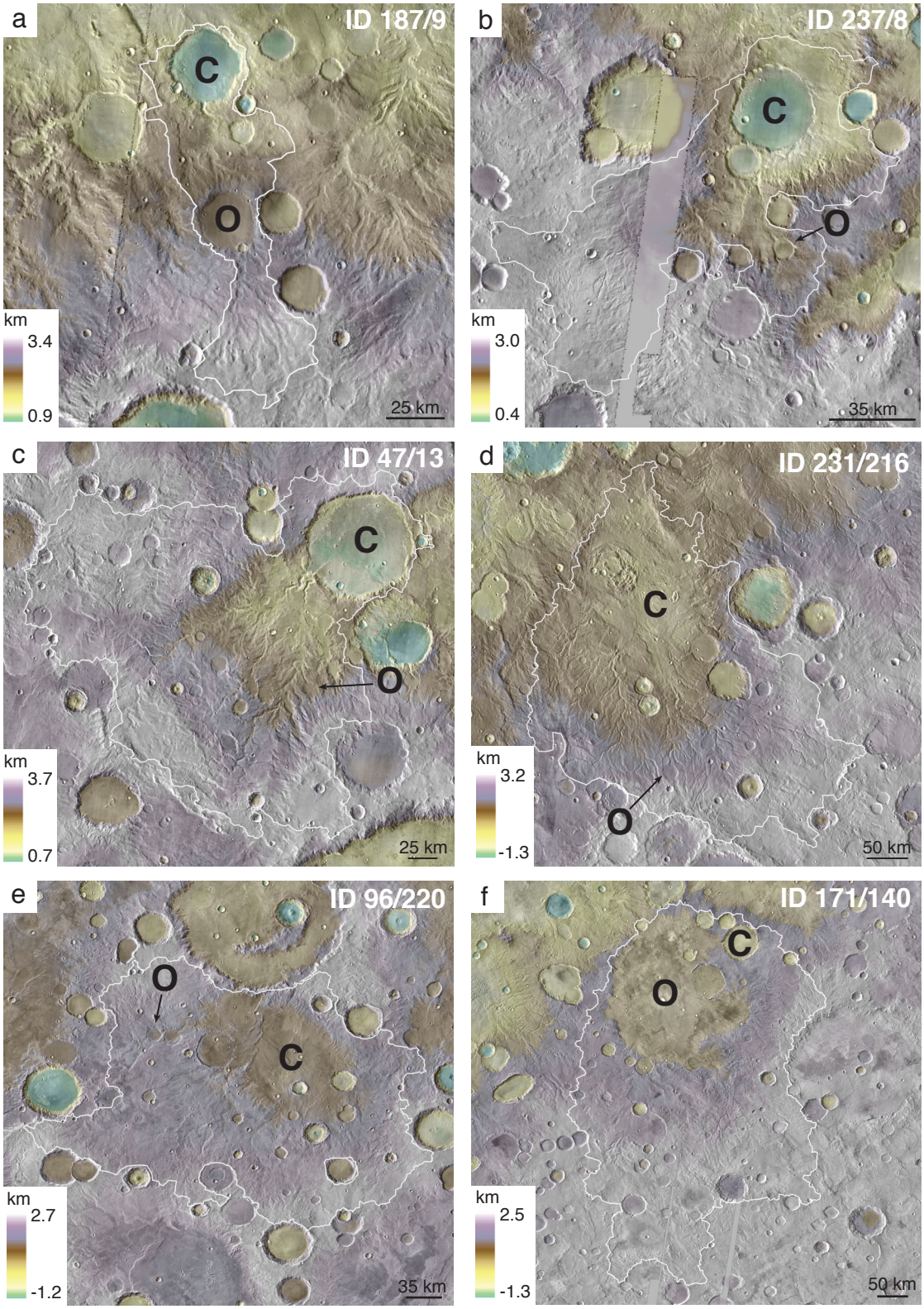

Figure S2. Coupled lake systems identified on Mars (excluding ID 185/89 in Figure 2a). O = open-basin lake; C = closed basin lake; white polygon = combined watershed and lake areas of each coupled system (Table S3). Elevation and images from MOLA and THEMIS, respectively.

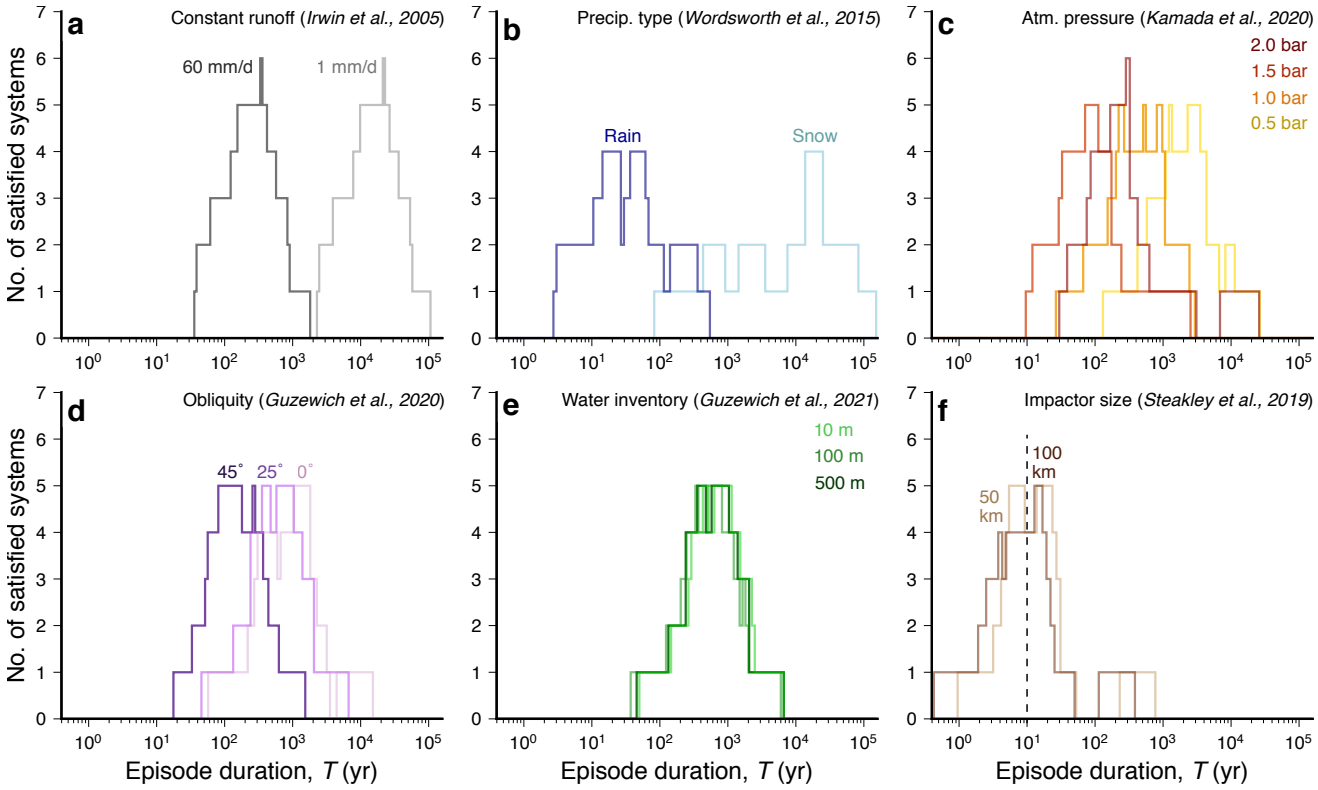

Figure S3. Distribution of runoff episode durations (assuming no evaporation; E=0) that satisfy the 7 studied coupled systems using different runoff constraints. See Figure 4 in main text for comparison and further details (where aridity index, AI = 0.26).

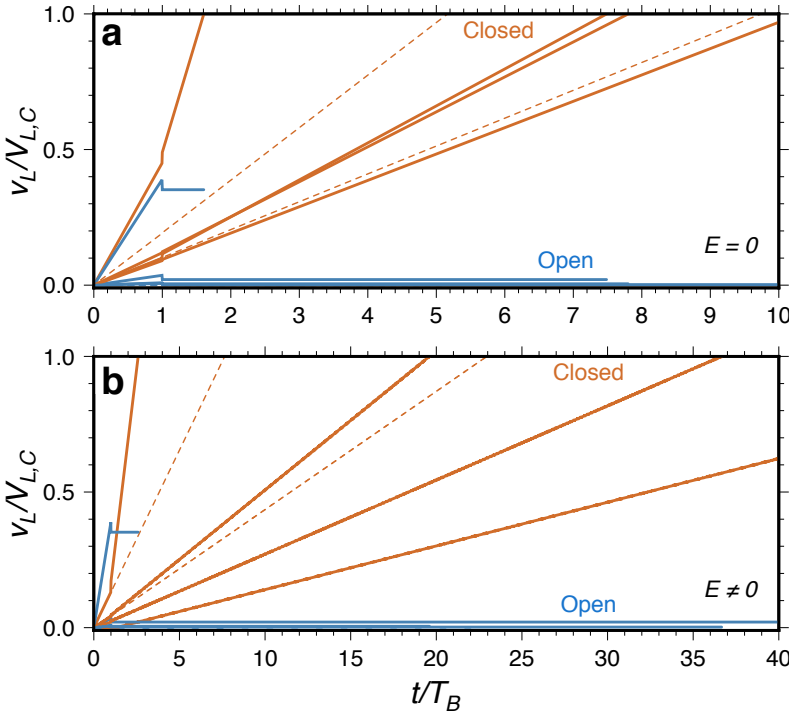

Figure S4. Lake volume changes over time (analogous to Figure 2e,f), but excluding two systems: Basin IDs 47/13 and 231/216 (shown in dashed lines; see Supplementary Text S1 for discussion; Table S3; Figure S2). Note that the total range of T_{max}/T_B remains unchanged. See Figures 2e,f for additional details.

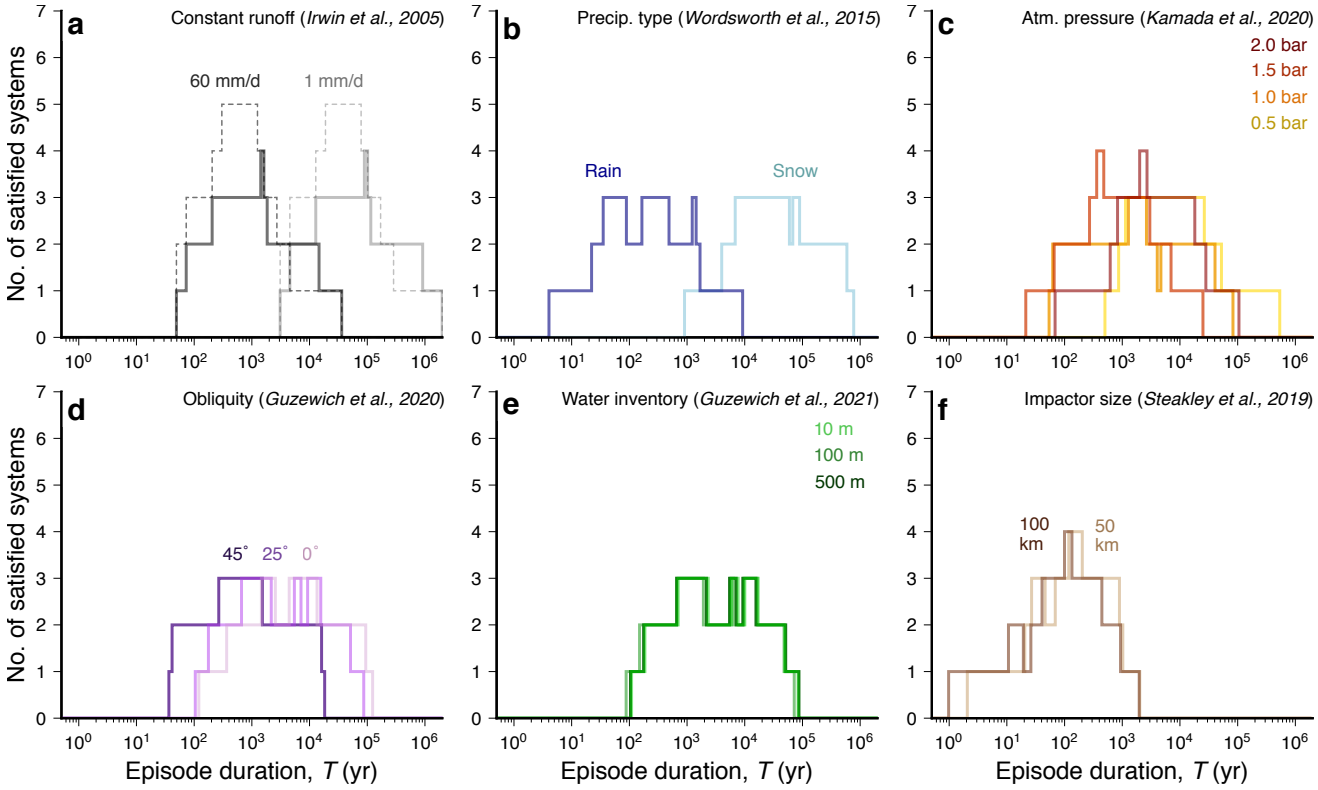

Figure S5. Distribution of runoff episode durations that satisfy 5 of the studied coupled systems using different runoff constraints. Here we exclude two systems: Basin IDs 47/13 and 231/216 (see Supplementary Text S1 for discussion; Table S3; Figure S2). Note that the new maximum is now 5. Dashed distributions in (a) show original distributions from Figure 4 for comparison. See Figure 4 in main text for further details (where all 7 coupled systems are considered). Note that location of peaks is similar to Figure 4.

Table S1. Water availability rates and their data sources. Minimum and/or maximum values are shown below in the format they were published in (before converted to an order of magnitude estimate in mm per Earth year for Figure 1 in the main text). Rates/studies are listed in the same order as Figure 1. When min/max results were not explicitly stated or tabulated, these were estimated from scale bar ranges provided in figures. Specific location of data in the original publication is indicated in the final column. For the models where the xy-data was made available (indicated with an asterisk), or geological runoff constraints where all results were tabulated and provided, we also present those results in Table S3.

Rate	Study	Data location
$8 - 3000$ m in 10^6 yr	Fastook et al. (2015)	Table 1; Figs. 7-12 (b,f,j)
$-2 - 0.5$ $\log_{10}$(kg/m^2/avg.) in 5 years	Wordsworth et al. (2015)*	Fig. 5a
$0.009 - 1.26$ cm/yr	Urata et al. (2013)	Table 4
$0 - 33$ kg/m^2 in 40 years	Wordsworth et al. (2013)	Figs. 4, 6, 7, 10
$0 - 3$ $\log_{10}$ of mm/yr	Kamada et al., (2020)*	Fig. 8
$0.001 - 1$ mm/day	Von Paris et al., (2015)	Abstract/Fig. 8
$< 10^-4 - 10^-2$ mm/hr	Scanlon et al. (2013)	Section 3.1
$0 - 40$ mm in a year	Palumbo et al. (2018)	Section 3.3.2/Fig. 11
$-1 - 0.5$ $\log_{10}$(m/yr/avg.)	Wordsworth et al. (2015)*	Fig. 4b
$30mm - 2.4$ m in a year	Ramirez et al. 2020	Figs. 11,12
< 100 mm/yr	Guzewich et al. (2020)*	Fig. 2
$1.5 - 10.6$ mm/day	Von Paris et al. (2015)	Table 1/Section 2.2.3
$0.7 - 9.69$ mm/day	Ramirez et al. (2020)	Table 1
$0.23 - 5.84$ m in one year	Steakley et al. (2020)*	Abstract
$0.1 - 6$ cm/day	Irwin et al. (2005)	Table 1
< 100 cm/yr	Soto et al. (2010)	Fig. 1B
$0.001 - 5$ cm in a southern winter	Mischna et al. (2003)	Figs. 6, 8, 10
$0.4 - 63$ cm/d	Hoke et al. (2011)	Table 3
< 0.14 m/day	Scanlon et al. (2016)	Section 3.1
$< 2 - 3$ mm/hr	Kite et al., (2013)	Section 8.5

Table S2. Precipitation/runoff constraints on early Mars from select previous studies. Figure 1 in the main text and Table S1 provide an order of magnitude overview of various studies (n=21), but here we provide additional details for 8 studies for which the data were made available to the authors. Rates from each study are expressed as the logarithmic mean and standard deviation ($\mu^{+\sigma}_{-\sigma}$) of provided datapoints[a]. The last column lists the number of runoff/precipitation datapoints from each study, as well as the percent of area of Mars that is covered.

Rate (mm/yr)	Type	Study	Data points (coverage)[a]
Local geological constraints:			
2378^{+4806}_{-1591}	Peak runoff	Irwin et al. (2005)	15 (0.7%)
6472^{+9850}_{3906}	Peak runoff	Hoke et al. (2011)	7 (0.5%)
1394^{+1185}_{-641}	Runoff	Von Paris et al. (2015)	18 (<0.1%)
848^{+1217}_{-500}	Runoff	Ramirez et al. (2020)	8 (0.1%)
Global climate models:			
81^{+1067}_{-75}	Rainfall	Wordsworth et al. (2015)	2185
$800^{+587}_{-339}; 3582^{+8300}_{-2502}$	Precipitation	Steakley et al (2020)[b]	2100
$10^{+12}_{-5}; 40^{+61}_{-24}$	Precipitation	Guzewich et al. (2020)[b]	3312
$3^{+4}_{-2}; 46^{+494}_{-42}$	Precipitation	Kamada et al. (2020)[b]	2048

[a] For global climate models, spatial coverage ∼100%, and datapoints correspond to the number of data nodes in each model grid. [b] For models that consider more than one climate scenario, we provide both minimum and maximum runoff scenarios.

Table S3. List of 7 coupled lake systems on Mars used for this study (originally identified in Stucky de Quay et al., 2020). Each row corresponds to a single coupled system, providing details on both the open- and closed-basin lake morphological parameters. The system type indicates whether it as an embedded (E) or adjacent (A) system (see main text for description).

Open-basin lakes (O)							Closed-basin lakes (C)						Type
Basin ID	Lat. (°)	Long. (°)	Lake Area, $A_{L,O}$ (m^2)	Lake Volume, $V_{L,O}$ (m^3)	Watershed Area, $A_{W,O}$ (m^2)	Remaining Lake Volume, V_R (m^3)	Basin ID	Lat. (°)	Long. (°)	Lake Area, $A_{L,C}$ (m^2)	Lake Volume, $V_{L,C}$ (m^3)	Watershed Area, $A_{W,C}$ (m^2)	
187	-7.2	43.0	672583920	70758474568	2693891297	63762980452	9	-5.8	42.8	937334813	181170078070	2951851160	E
[a]231	7.8	47.8	71349069	2214100227	922578879	1213230624	216	11.2	47.3	16423192980	1999070439438	74750868307	E
185	2.2	45.5	153020661	12052978646	1347895789	6879905806	89	3.0	45.5	1195725678	331637791895	2933305480	E
237	-4.4	88.4	42189599	3528718923	835736020	2054182263	8	-3.3	88.3	2159319657	393910203622	9585477072	E
[a]47	-10.4	128.0	84149421	6328284206	542604498	555988086	13	-8.3	128.7	10474531739	3158342140525	49459904633	E
96	-29.8	147.2	201164702	11882850022	4501243923	4375182735	220	-30.1	149.7	13702674269	1831669964644	52016978068	E
171	-21.3	-5.3	51471447808	7549380842062	176743110693	1035198695083	140	-19.9	-2.9	3437356502	1464448780733	10626445666	A

[a] Coupled systems removed from consideration for Figures S4 and S5. See Supplementary Text S1 for more information.

Table S4. Summary of all model outputs used in this work, with a total of 16 scenarios from four climate model studies.

Study/Model	Scenario	Location in Figure 4
Wordsworth et al. (2015)	Rainfall (1 bar, solar flux=764.5 W m^{-2})	b (rain)
	Snowfall (0.4 bar, solar flux=441.1 W m^{-2})	b (snow)
Kamada et al., (2020)	0.5 bar	c (0.5 bar)
	1.0 bar	c (1.0 bar)
	1.5 bar	c (1.5 bar)
	2.0 bar	c (2.0 bar)
Guzewich et al. (2020)	10 m GEL[a], obliquity=25°	d (25°) & e (10 m GEL)
	10 m GEL, obliquity=45°	d (45°)
	10 m GEL, obliquity=0°	d (0°)
	100 m GEL, obliquity=25°	e (100 m GEL)
	100 m GEL, obliquity=0°	-
	500 m GEL, obliquity=25°	e (500 m GEL
Steakley et al., (2019)	1 bar, 50 km-impactor, RAC[b]	f (50 km)
	1 bar, 50 km-impactor, RIC[b]	-
	1 bar, 100 km-impactor, RAC	f (100 km)
	150 mbar, 100 km-impactor, RIC	-

[a]GEL = global equivalent layer; [b]RAC = radiatively active clouds; RIC = radiatively inert clouds.